Pulsating Magnetospheric Field-Aligned Electrons

C.E. McIlwain, S.S. Kerr

Center for Astrophysics and Space Sciences, University of California, San Diego, 9500 Gilman Drive, La Jolla, CA, USA 92093

Abstract

The Electron Drift Instruments (EDI) on the Cluster spacecraft are often operated in a mode that measures electron fluxes simultaneously parallel and anti-parallel to the magnetic field, at energies of 500 or 1000 eV. In the burst mode, accumulations are made 128 times per second. Spectrograms made using wavelet techniques covering the frequency range of 0.001 to 64 Hz reveal pulsations in many frequency bands. These pulsations extend from below the Pc-5 band up to and past the Pc-1 frequency band. Often, one direction dominates for a short period, thus indicating the presence of a field-aligned current filament. Individual accumulations are sometimes 50% higher than their neighbors less than 8 ms away. These fast pulses may be due to the passage of electron solitons travelling along the current filament.

Key words: Cluster, beams, solitons, vortices, aurora

1 Introduction

Active plasma processes can generate intense beams of electrons that travel to distant regions of the magnetosphere. The electron beams first observed at very high altitudes (McIlwain, 1975) exhibited large, rapid fluctuations. These fluctuations provide important clues about the beam-acceleration processes and about the processes generated by the beams as they travel along magnetic-field lines.

The EDI instruments on the Cluster spacecraft provide a unique opportunity to study the character of these beam fluctuations, by taking measurements of ambient particle fluxes at a frequency of up to 128 times per second at selected pitch angles.

2 Instrumentation

The Electron Drift Instruments (EDI) can obtain measurements of the electric field $\mathbf{E}_\perp$ as well as the gradient of the magnitude of the magnetic field $\boldsymbol{\nabla}_\perp B$, both in the plane perpendicular to the magnetic field $\mathbf{B}$. EDI emits a weak beam of electrons from the supporting spacecraft and measures the drift of these electrons, as they gyrate one or more times in the plane perendicular to $\mathbf{B}$ before returning to detectors on the spacecraft. The details of EDI design and operation have been reported by Paschmann et al. (1997), Paschmann et al. (1998) and Vaith et al. (1998).

In order to measure the electron drift continuously and independently of the spacecraft spin phase, EDI must employ two oppositely-oriented detectors, each of which can be directed electronically to view over a full 2π sr. These detectors have tunable energy bandpass and acceptance angle, and achieve high sensitivity via 'double-angle' focussing of particles that enter the detector aperture. With its electron guns turned off, EDI then becomes a highly capable detector of ambient particle distributions in selected regions of phase space. Since real-time *in situ* measurements of the local magnetic-field vector are available to EDI, these regions of phase space may be examined with respect to the magnetic field at high time-resolution, independently of the spacecraft spin phase.

EDI was launched on all four of the Cluster spacecraft in 2000 and is operating currently on three of the spacecraft. The measurement of electron drift is carried out by emitting and detecting electrons with energies of 500 eV or 1 keV. When operated in an 'ambient' mode, the EDI detector can measure ambient particle fluxes at these same energies and at pitch angles of 0°, 90° and 180°. The angular resolutions of these measurements are mode-dependent, and are typically $15^\circ \times 30^\circ$ for the data analyzed in this paper. Although the EDI detectors are able to measure ion fluxes, only electron fluxes have been measured to date. Depending on the telemetry mode, count samples are supplied from both detectors once every 64 ms or 8 ms.

Data obtained using this 'ambient' mode while in the magnetotail, reveal frequently the presence of electron beams (Runov et al., 2004; Asano et al., 2005). The on-board EDI ambient-mode software was modified in the fall of 2004 to improve accumulation times, duty factors and detector-response antenna patterns. The EDI data discussed in this paper take advantage of these improvements.

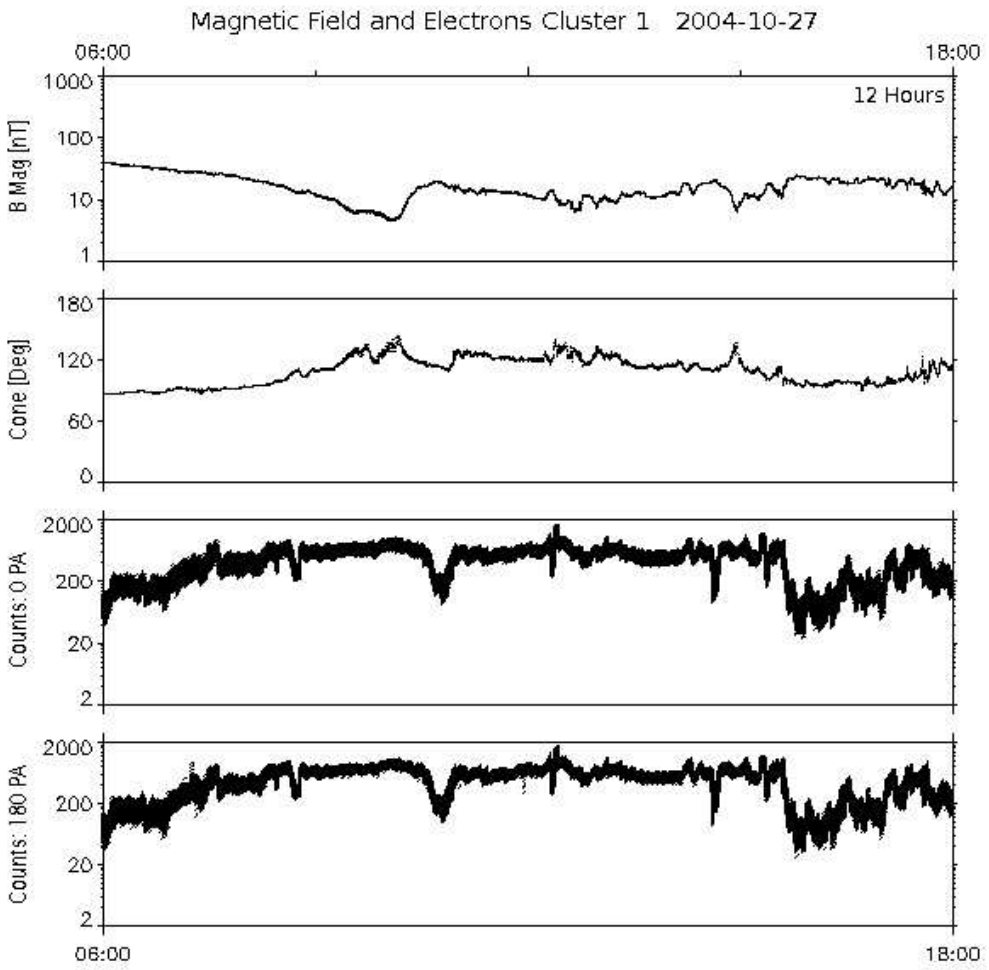

Fig. 1. Plots of the FGM magnetic-field magnitude and cone angle, and the parallel and anti-parallel 0.5 keV electron count data from EDI on Cluster spacecraft 1 (C1) for the 6 to 18 UT time period on Oct. 27, 2004. During this period, C1 was near $L = 17$ and magnetic local time 21 h. The K_p values varied from 0 to 2^-.

3 Quiet Magnetotail

Figure 1 shows an example of 0° and 180° pitch-angle electron count data gathered on 2004/10/27 06:00–18:00 UT by the EDI detectors on Cluster spacecraft 1 (C1) with the ambient mode described above. Also shown are the magnitude of the magnetic field B and its cone angle with the spacecraft spin axis. Figure 2 'zooms' from 12 h to 20 min and to 1 min intervals for the 180° data shown in figure 1. Few variations with time scales less than one minute are present during this quiet time period. The apparent increased thickness of the plots at the longer time scales is due to the horizontal compression of the plot points and the consequent increase in density of variations over time scales larger than one minute.

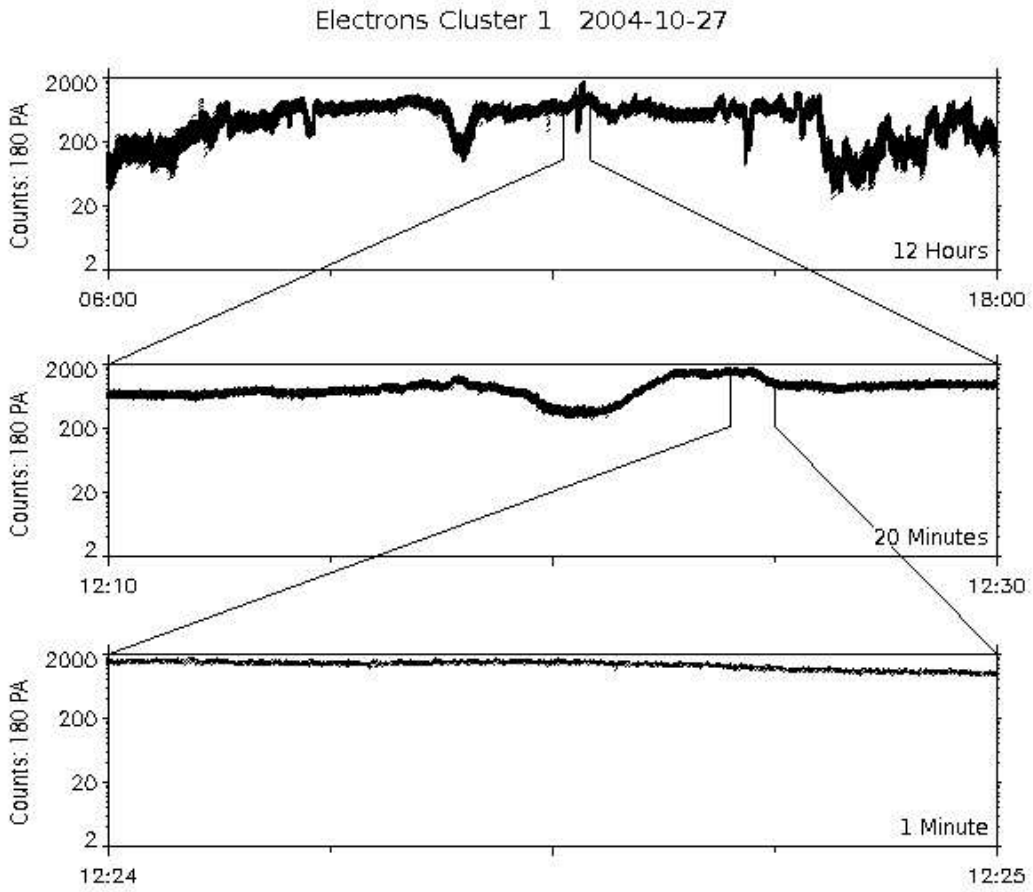

Fig. 2. The anti-parallel count data from figure 1 over time periods of 12 h, 20 min and 1 min. Note the relative absence of fluctuation on time scales of less than one minute.

These data are shown as count rates per accumulation interval and have been corrected for variations in the response of the EDI detector as a function of the polar and azimuthal look-directions in the detector's reference frame.

4 Wavelet Analysis and the Use of Colour

The EDI ambient electron-count rates were analyzed as a time series with spacing δt, equal to 0.0625 s (16 Hz) for the 'nominal' telemetry mode (NM) and 0.0078125 s (128 Hz) for the 'burst' mode (BM). Wavelet techniques were employed as described by Torrence and Compo (1998) and implemented in software provided with the Interactive Data Language (IDL) package, available commercially from Research Systems Incorporated (RSI). Morlet wavelets of

the following form

$$\psi\left[\frac{(n'-n)\delta t}{s}\right] = \left(\frac{\delta t}{\sqrt{\pi}s}\right)^{\frac{1}{2}} \exp\left[\imath\omega_0\frac{(n'-n)\delta t}{s}\right] \exp\left[-\frac{((n'-n)\delta t)^2}{2s^2}\right] \quad (1)$$

were used exclusively. Here n is a localized time index, s is the scale parameter (units of time) used to modify the sample band of the wavelet, and ω_0 is the 'nondimensional frequency' parameter. Wavelet transforms $W_n(s)$ of the data over a sequence of scale factors s and a chosen ω_0 are obtained by convolving the above wavelet formula with the data time series over the n' index. Practical values of ω_0 are chosen typically to be no less than 3, and preferably 6 or higher, in order to satisfy nominally the two wavelet 'admissibility conditions' of zero mean and localization in time and frequency space. A sinusoidal signal at the fourier frequency $(\omega_0 + \sqrt{2+\omega_0^2})/4\pi s$ yields maximum power in the wavelet spectrum when transformed with a Morlet wavelet of scale s; it is this frequency that is used to label the spectra shown below.

Because Morlet wavelets are complex-valued, they can provide phase as well as amplitude information about the time-frequency spectrum. Therefore they are useful for displaying the relative phase in the spectra of two data sets, such as the electron fluxes measured by EDI simultaneously in two opposite directions. In addition, EDI data can be compared in this way with EDI data from other spacecraft, or with data from other instruments on the same spacecraft.

The task of analyzing a high-resolution dataset with such a large number of dimensions has motivated the authors to develop and employ a visualization technique based on colour overlays. In addition to assigning two parameters (e.g., time and frequency) to the horizontal and vertical dimensions of a typical display medium, we have assigned the three colour components (red, green and blue) to three parameters related to the spectral data.

For example, figure 3 displays EDI ambient electron data with the amplitude of the 0° spectral data assigned to the blue channel, the 180° to the green channel and the relative phase of these two spectra (scaled to amplitude) to the red channel. With the data thus assigned, an equal electron flux in both pitch angles with 180° relative phase will appear as a shade of gray. Therefore, an abundance or absence of any of the three colours would indicate an anisotropy or a variation in relative phase, or both. Specifically, cyan reveals the presence of green and blue together (or equivalently the absence of red) indicating equal fluxes in phase. Similarly, magenta (or yellow) reveals an anisotropy with an abundance of 0° (180°) flux that is out of phase with its 180° (0°) counterpart. All other colours indicate various contributions from the three data channels.

While this method of presenting phase or flow features in the spectra lacks the quantitative precision of other methods such as hodograms or 'clock-hand'

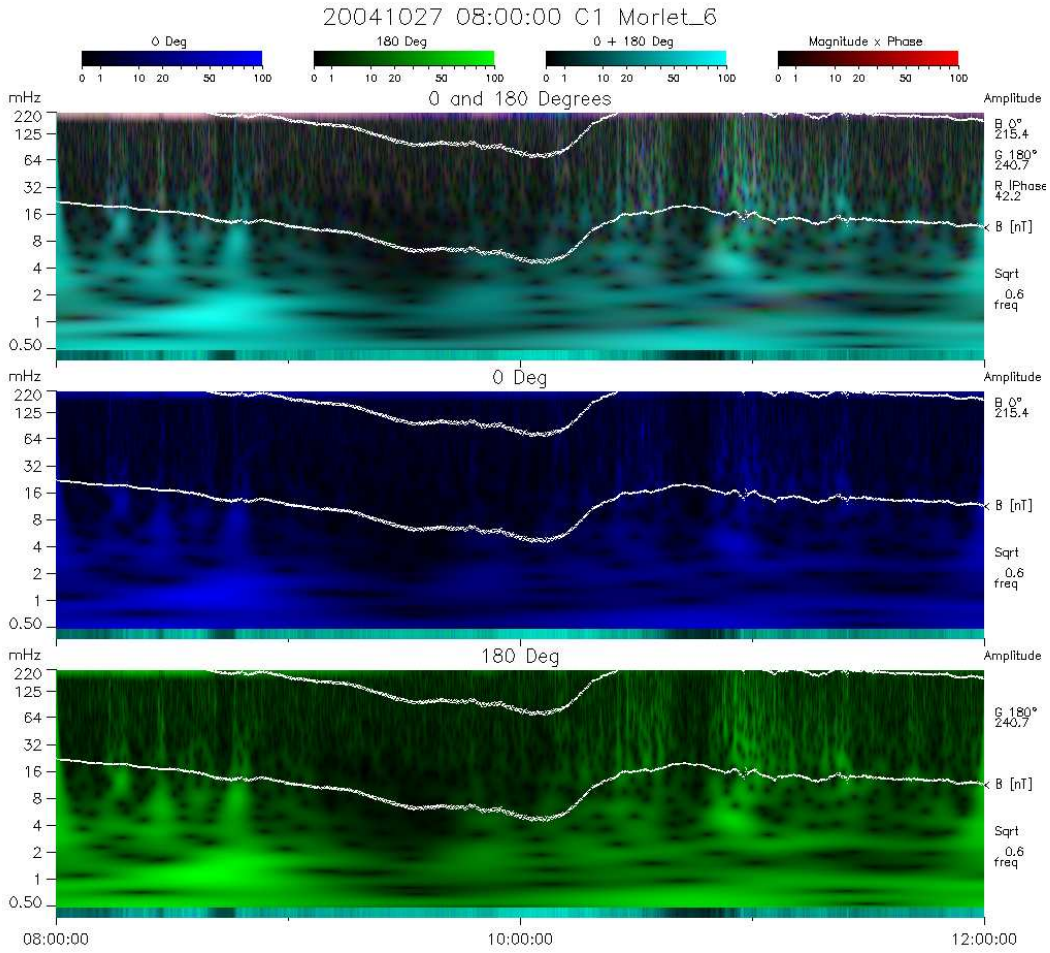

Fig. 3. The spectrum of the parallel 0.5 keV electrons is shown in green in the bottom panel for the 8 to 12 UT time period, the anti-parallel spectrum in blue in the middle panel, and the combined spectra in the top panel along with their magnitudes times the relative phase in red. The lower white-line plot is the magnitude of the magnetic field in nT and the upper white line is the proton gyrofrequency in mHz.

vector fields, it offers the advantage of higher resolution and contrast for these features in frequency-vs-time spectral images. The visibility of spectral features is enhanced by flattening the spectra by a power-law frequency dependence.

Figure 3 shows 0.5–220 mHz spectral data from 08:00 to 12:00 UT for the same day and spacecraft as for figures 1 and 2. The use of colour in the 0°, 180° and 0°+180° panels is illustrated. The similarity of the spectra for the two directions is revealed by the absence of blue and green in the top panel. Note also the 1 and 2 mHz lines in both the 0° and 180° pitch-angle spectra from 11 to 12 UT.

In figure 4, the 0°+180° combined spectral data (0.5-220 mHz) from Cluster spacecraft 1, 2 and 3 are displayed together to facilitate comparison. Again,

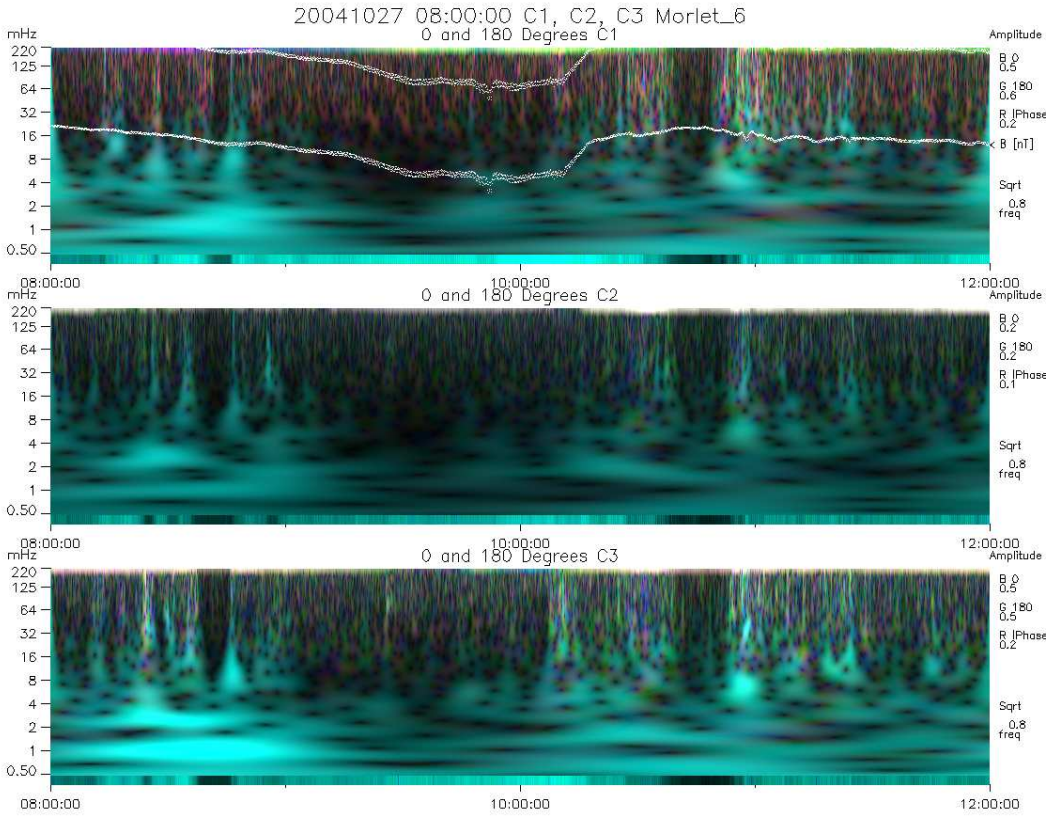

Fig. 4. The EDI ambient electron spectra from Cluster 1, 2, and 3 for the same time interval as figure 3. Note that the spectra show many similarities even though the spacecraft are separated by about 1000 km.

note the relative absence of blues and greens, as well as the similarities between spacecraft.

Figure 5 shows 0.5–125 mHz spectral data from EDI and the on-board fluxgate magnetometer (FGM) overlaid with colours to display relative power and phase. The spectra of the magnitude of the magnetic field is shown in blue, and the $B_\perp$ spectra (created from the cross products with the vector field at the mid-time of the plot) is shown in green. Note that there are similarities between the electron and magnetic-field spectra in addition to the strong differences such as the rise in perpendicular fluctuation of B from 10:00 to 10:05 in the range from 3 to 32 mHz, with no companion feature in the electron spectrum. The magnetic-field values shown here are from the spin-averaged prime parameters. Future studies are planned that will use B-field values of higher time resolution.

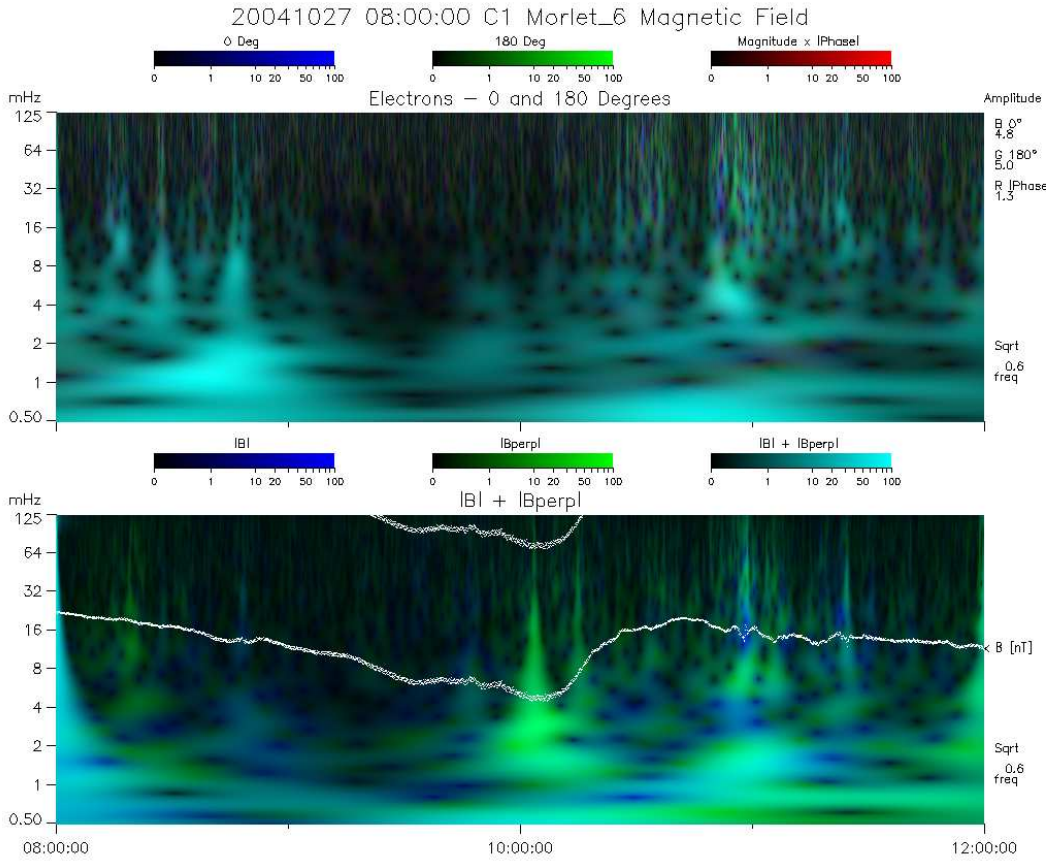

Fig. 5. EDI ambient electron and FGM spectra from 8 to 12 UT on Oct. 27, 2004. The spectra of the spin-averaged magnetometer data shown in the bottom panel has few features that match the electron pulsations. The modulation of these electrons traveling along the magnetic field likely occurs at some distance from the spacecraft.

5 Disturbed Magnetotail

Figure 6, shows the B field and the EDI ambient electron count data as Cluster 1 went from $L = 14.4$ to $L = 17.8$ at a local time of about 20 h during a very disturbed period. For over 3 hours in the initial part of this period, the magnetic field remained relatively stable, while the electron count rates exhibited strong and rapid fluctuations.

Figure 7 displays successively shorter time intervals of the 180° pitch-angle data, from the same 12-hour time period as shown in figure 6. The bottom two panels show the 180° and 0° data over a 10 s interval, in which the 180° data exhibited multiple sharp peaks while the 0° data was relatively constant. These data were gathered with EDI operating in the nominal telemetry mode, with 16 samples taken every second, each over an accumulation time of 15.6 ms. The strong time-variations evident in these peaks may be from variations beyond the 8 Hz Nyquist frequency. The 15.6 ms accumulation time gives a substantial

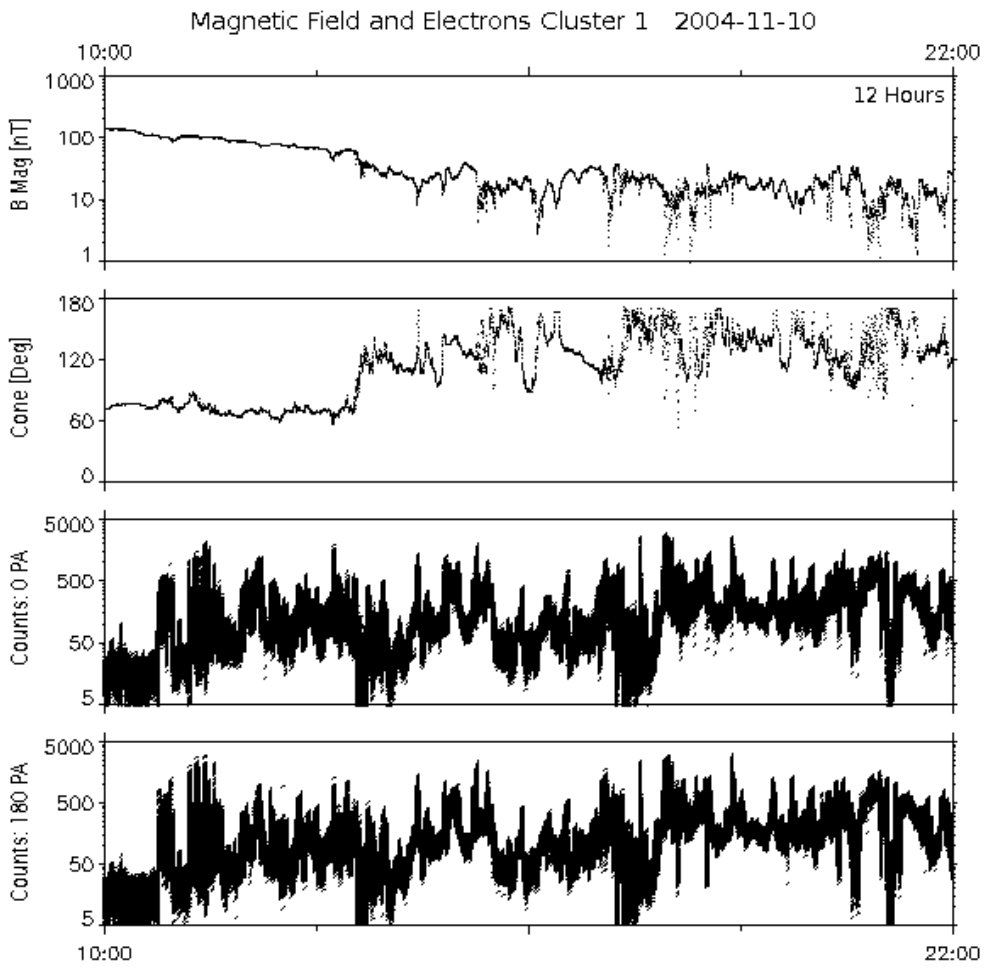

Fig. 6. FGM B-field and EDI electron-count rates in the magnetotail with K_p values ranging from 7^+ to 4^+ during a 12-hour period on Nov. 10, 2004. Note that the magnetic field remained relatively stable during the initial part of this period, while the electrons exhibited strong, rapid variations.

response up to 50 Hz and higher.

The top panel of figure 8 displays the colour-overlaid wavelet spectra of the 0° and 180° fluxes and their relative phase. for the 60-minute interval shown in the second panel of figure 7. The bottom panel shows the overlaid spectra of the B and $B_\perp$ data and their relative phase. (See above for the definition of $B_\perp$.)

6 Magnetopause and Cusp near Perigee

Earlier on Nov. 10, 2004, Cluster spacecraft 2 (C2) was operating in the burst mode as it approached the magnetopause/cusp near perigee at less than 5 R_E

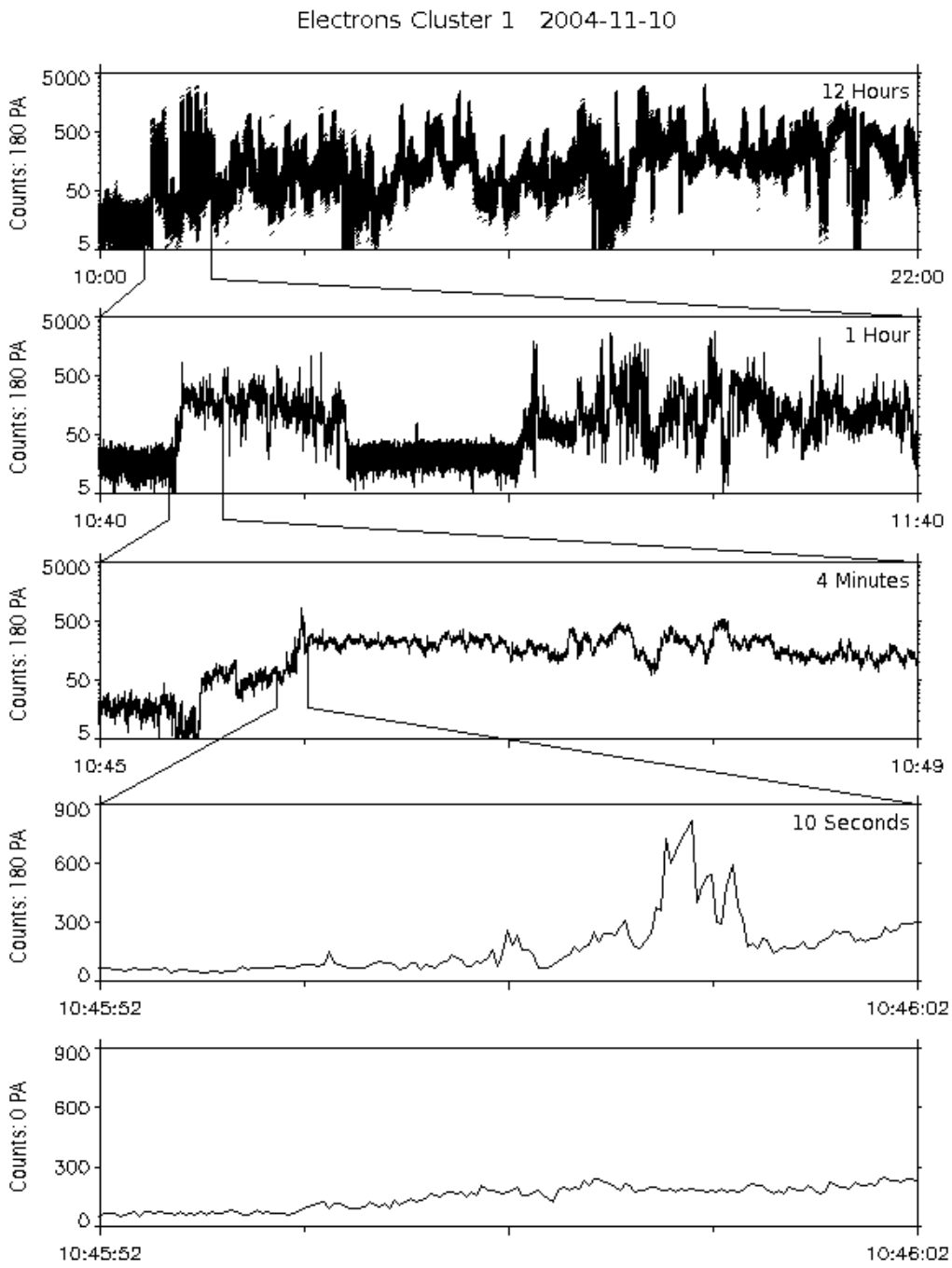

Fig. 7. EDI 180° pitch-angle electron count data from C1 over the same 12 h period shown in figure 6, with zooms to 1 h, 4 min, and 10 s. The bottom panels shows the 0° data for the same 10 s interval. Note the differences and the multiple peaks in the 180° pitch-angle data that are likely due to undersampled fast time variations.

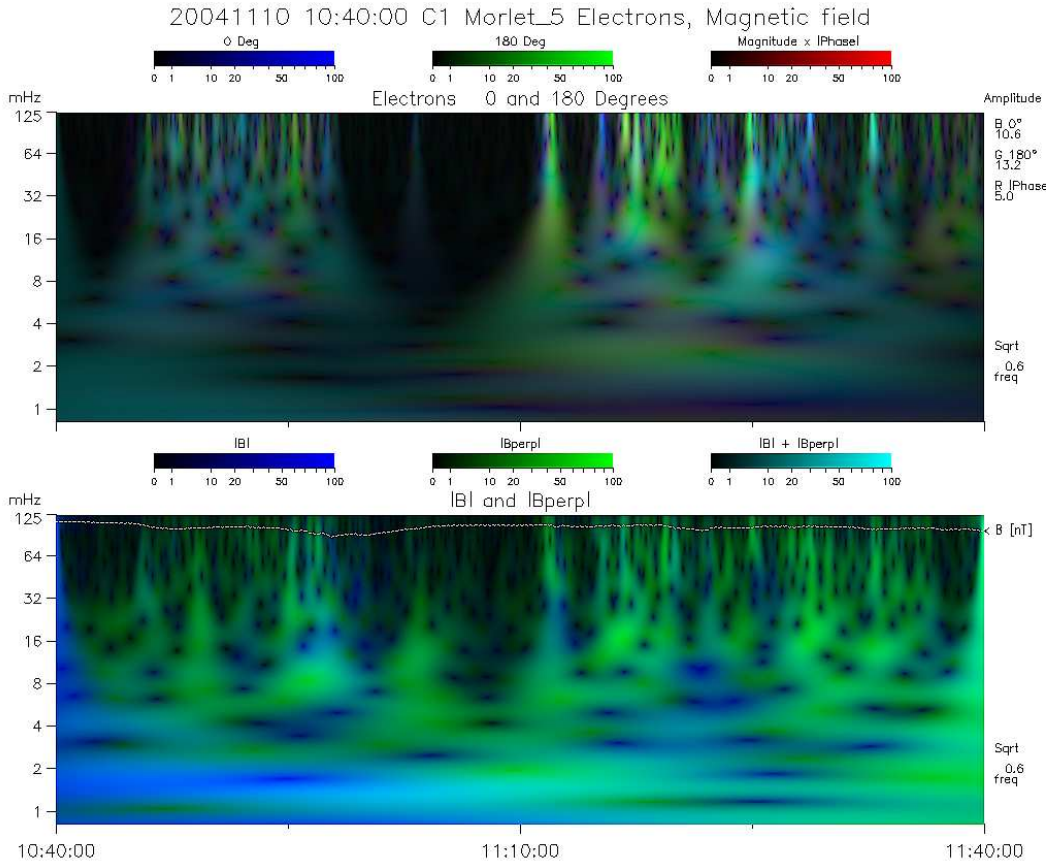

Fig. 8. Spectra of the 0° and 180° pitch-angle EDI electron count data for the same 60 m interval as the one shown in the second panel of figure 7. The lower panel shows the spectrum for the magnetic field during the same interval.

at a magnetic local time of 9 h, while $K_p = 8^+$.

Figure 9 presents line plots over 50 min, 4 min, 40 s, 8 s and 2 s of 0° pitch-angle data at energy $W = 500$ eV. A sharp spike that occurred at 04:42:59.5 over a 7.8 ms accumulation time is marked with an arrow. It is possible that this spike is due to a field-aligned packet of electrons driving a soliton past the spacecraft. The accumulation time of 7.8 ms times the velocity of a 500 eV electron corresponds to a packet length of 100 km or less. For a beam narrower than the detectors' acceptance angle of $15° \times 30°$, the effective area times the efficiency is about 0.4 cm^2. The observed peak of 3135 counts in 7.8 ms would thus correspond to 10^6 electrons $\mathrm{cm}^{-2}\mathrm{s}^{-1}$ or 1.6 $\mathrm{nA\,m}^{-2}$ within the detectors' energy pass-band of about 460 to 540 eV.

Figure 10 shows the overlaid EDI ambient electron spectra for the 50 min time period shown in figure 9, along with the overlaid B-field spectra. During this period, the magnitude of B varied between 554 and 614 nT. In the top panel is a 48 s detail of the overlaid electron spectra that includes the time of the spike in the 0° pitch-angle flux, marked with a down-caret in both panels. This

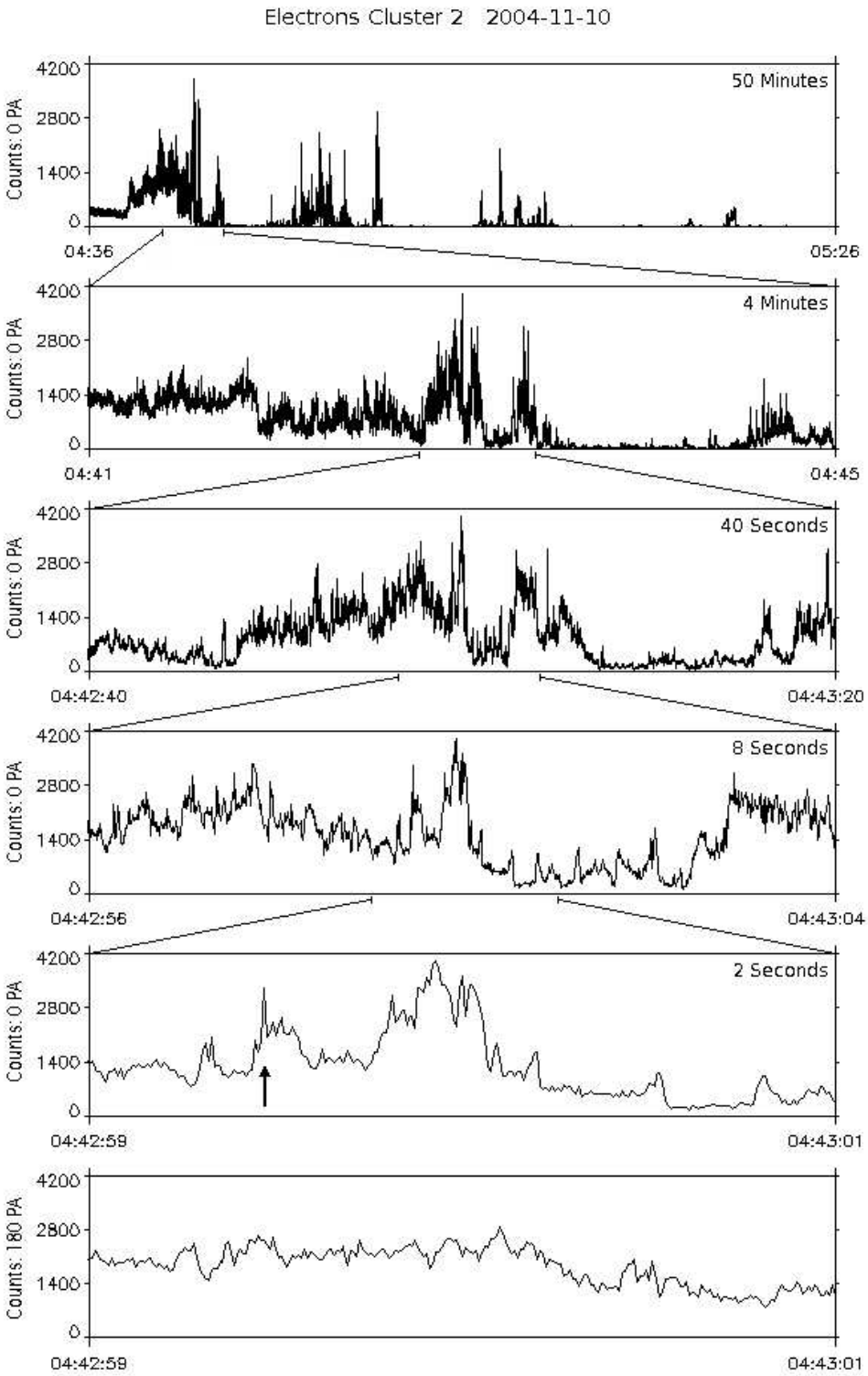

Fig. 9. EDI 0° pitch-angle electron count data from C2 on Nov. 10, 2004, showing successively smaller time intervals from 50 min to 2 s. The bottom panel shows the 180° data for the same 2 s time period. The arrow marks the sharp (within 8 ms!) spike at 04:42:59.5 UT. C2 was near perigee ($R = 4.4$, $L = 8$, LT= 8.8).

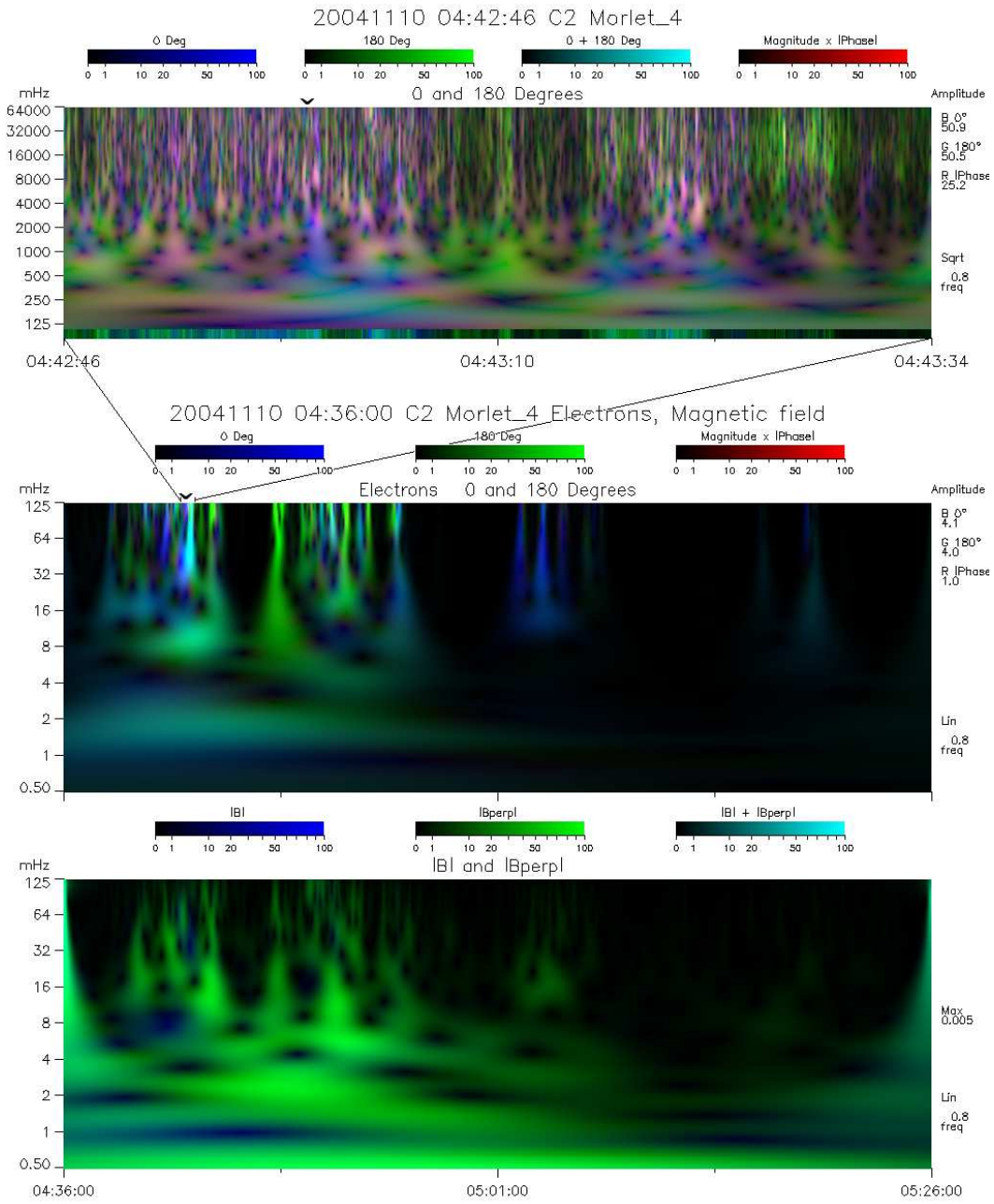

Fig. 10. The lower two panels show EDI ambient electron and FGM B-field spectra from 0.5 mHz to 125 mHz for the same 50 min time period shown in figure 9. The upper panel shows the combined 0+180+phase spectra from 125 mHz to 64 Hz for a 48 s interval that overlaps nominally with the 40 s interval shown in figure 9. The spikes in the 0° at 04:43 appear in the spectra as a region of blue in the range 0.5–2 Hz.

48 s spectrogram barely resolves the entire 2 s line plot which, in turn, barely resolves the spike. Fluctuations are visible up to the 64 Hz Nyquist frequency.

It is possible that Cluster 2 encountered vortices of the type discovered by

Sundkvist et. al. (2005) during this time period. These vortices may have been accompanied by electron-acoustic solitary waves involving beams of electrons, such as those discussed by Shukla et al. (2004).

It is also possible that these beams are associated with impulsive reconnection events (Bhattacharjee et al., 2005). High-time-resolution data produced by other Cluster instruments are being obtained and will be used to determine the nature of the processes in the vicinity of the spacecraft and in the beam-generation regions.

7 Magnetopause and Cusp at 11 R_E

On Jan. 25, 2005, Cluster 1 was operating in the burst mode as it approached the magnetopause/cusp during a quiet $K_p = 1$ period at $R = 11.3$, $L = 15.5$ and MLT=15.5. Figure 11 shows two bursts of field-aligned 500 eV electrons within a 30 s period. The first burst is predominantly anti-parallel, and the second is predominantly parallel. Both contain sharp peaks that are probably unresolved even with the 7.8 ms data-point spacing that EDI can achieve. Figure 12 shows the spectra of these two bursts. No discrete spectral peaks are revealed; only broad bands are visible near 3, 10 and 30 Hz.

These fast variations, as in other cases shown here, are probably associated with auroral acceleration processes (Bounds et al., 1999; McFadden et al., 2003; Ergun et al., 2004). Upward-travelling electron beams are observed regularly in the regions immediately above auroral displays, and it is usually assumed that beams observed beyond 4 R_E are also connected to auroras (McIlwain, 1975).

8 Discussion

There have been many observations of upward-travelling electrons at all local times by low- and medium-altitude spacecraft, most notably the FAST spacecraft (Carlson et al., 1998; Ergun et al., 1998; Pfaff et al., 1998). In order to understand the complex physical processes involved, the EDI observations at very high altitudes will need to be compared carefully with simultaneous data gathered from lower-altitude spacecraft (Deng et al., 2005) as they traverse nearby magnetic-field lines.

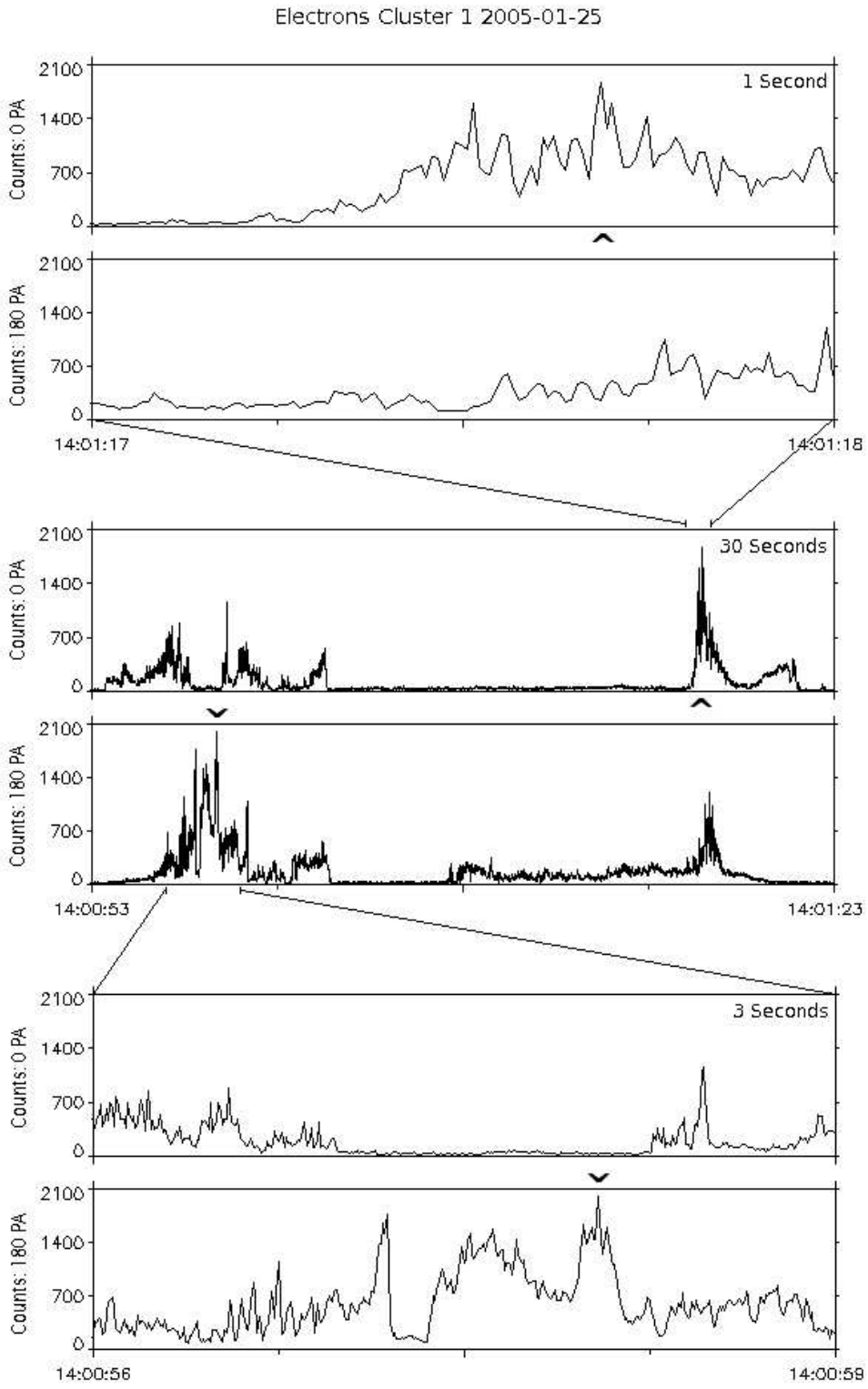

Fig. 11. A 30 s line plot of EDI ambient electron count data in the two middle panels with zooms to 3 s (1 s) intervals in the bottom (top) two panels. The peak in the 0° (180°) PA data at 14:01:17.68 (14:00:58.04) is marked with an up-caret (down-caret). The magnitude of the magnetic field varied between 22 and 32 nT during the 30 s interval of the middle panels.

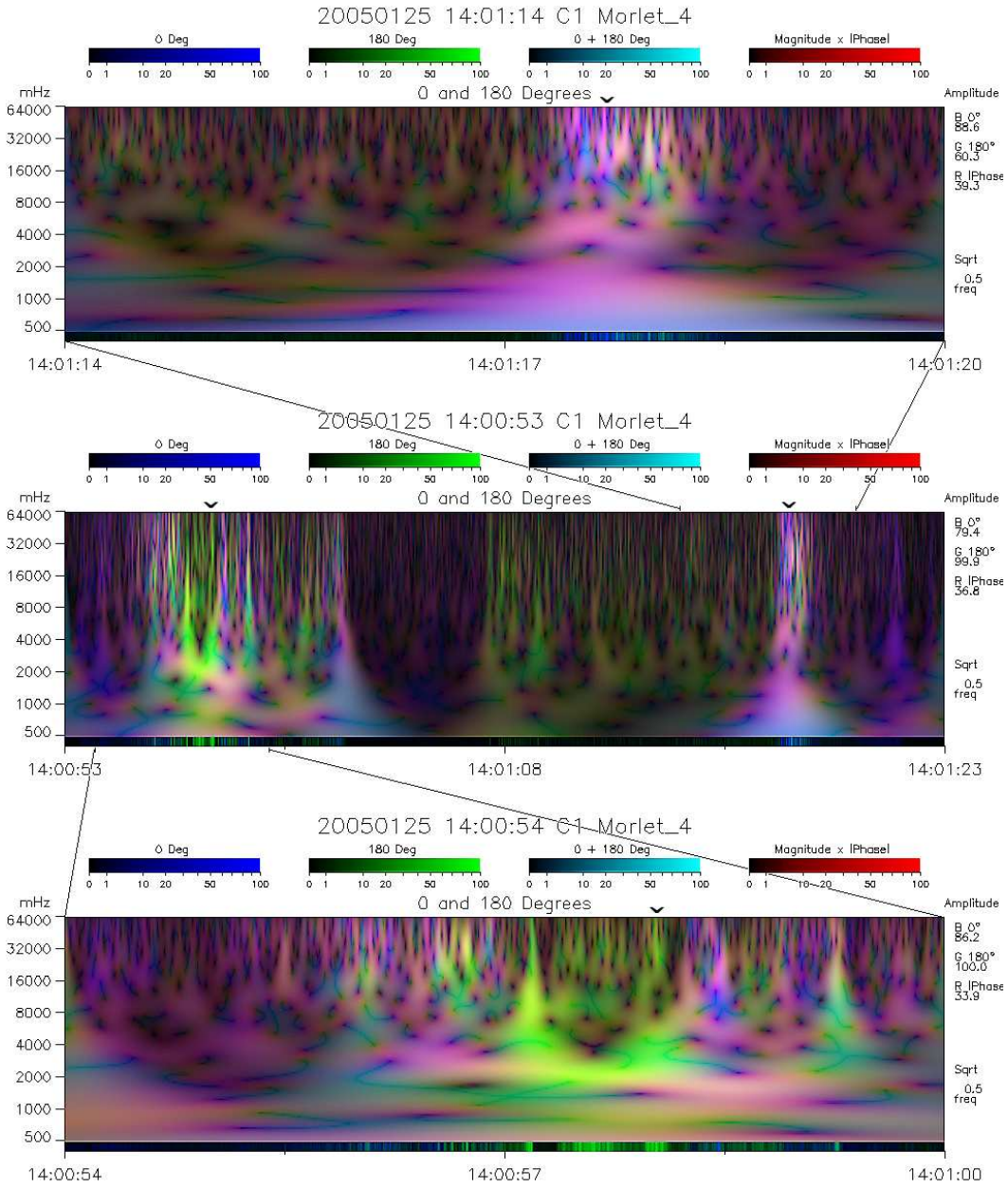

Fig. 12. Combined spectra for the same 30 s time period shown in figure 11 (middle panel), with spectra over 6 s time intervals containing the spikes in the 0° PA (upper panel) and 180° (lower panel).

9 Conclusions

The observations presented here of large fluctuations and the relative absence of periodic variations indicates the presence of turbulence generated by non-linear processes. Future studies using high-time-resolution electric- and magnetic-field data are expected to confirm the soliton origin of the observed packets of field-aligned electrons and their relationship to auroral acceleration

processes.

Acknowledgements

We are indebted to E. Howatt for developing much of the software used to process and display the wavelet spectra of the EDI data. We are also grateful to B. Yukich and X. Lee for their valuable assistance in the preparation of this paper, and to the other members of the EDI team for many insightful discussions. We acknowledge with thanks A. Balogh and E. Lucek for permission to use FGM data from CDAWeb in this paper, and M.A. Hapgood for providing data on the Cluster orbit and L values. We also thank the reviewers of this paper for their insightful comments and suggestions. This work was supported by NASA grant NNG04GA46G.

References

Asano, Y., Nakamura, R., Runov, A., Baumjohann, W., McIlwain, C., Paschmann, G., Quinn, J., Alexeev, I., Dewhurst, J.P., Owen, C.J., Fazakerley, A.N., Baloghf, A., Rème, H. and Klecker, B., 2005. Detailed Analysis of Low-Energy Electron Streaming in the Near-Earth Neutral Line Region During a Substorm. Adv. Space Res. 35. in press.

Bhattacharjee, A., Germaschewski, K., and Ng, C.S., 2005. Current singularities: Drivers of impulsive reconnection. Phys. Plasmas 12, 042305.

Bounds, S.R., Pfaff, R.F., Knowlton, S.F., Mozer, F.S., Temerin, M.A., and Kletzing, C.A., 1999. Solitary potential structures associated with ion and electron beams near 1 R_E altitude. J. Geophys. Res. 104, 28709.

Carlson, C.W., McFadden, J.P., Ergun, R.E., Temerin, M., Peria, W., Mozer, F.S., Klumpar, D.M., Shelley, E.G., Peterson, W.K., Moebius, E., Elphic, R., Strangeway, R., Cattell, C., and Pfaff, R., 1998. FAST observations in the downward auroral current region: Energetic upgoing electron beams, parallel potential drops, and ion heating. Geophys. Res. Lett., 25(12), 2017.

Deng, X.H., Tang, R.X., Nakamura, R., Baumjohann, W., Zhang, T.L., Daly, P.W., Rème, H., Carr, C.M., Balogh, A., Liu, Z.X., and Wang, J.F., 2005. Observation of reconnection pulses by Cluster and Double Star. Ann. Geophys. 23, 2927.

Ergun, R.E., Carlson, C.W., McFadden, J.P., Mozer, F.S., Delory, G.T., Peria, W., Chaston, C.C., Temerin, M., Roth, I., Muschietti, L., Elphic, R., Strangeway, R., Pfaff, R., Cattell, C.A., Klumpar, D., Shelley, E., Peterson, W., Moebius, E., and Kistler, L., 1998. FAST satellite observations of large-amplitude solitary structures. Geophys. Res. Lett., 25(12), 2041.

Ergun, R.E., Andersson, L., Main, D., Su, Y.-J., Newman, D.L., Goldman,

M.V., Carlson, C.W., Hull, A.J., McFadden, J.P., and Mozer, F.S., 2004. Auroral Particle Acceleration by Strong Double Layers: The Upward Current Region. J. Geophys. Res. 109(A12), A12220.

Lockwood, M., and Smith, M.F., 1992. The Variation of Reconnection Rate at the Dayside Magnetopause and Cusp Ion Precipitation. J. Geophys. Res. 97(A10), 14841.

McFadden, J.P., Carlson, C.W., Ergun, R.E., Mozer, F.S., Muschietti, L., Roth, I., and Moebius, E., 2003. FAST observations of ion solitary waves. J. Geophys. Res. 108(A4), 8018.

McIlwain, C.E., 1975. Auroral Electron Beams Near the Magnetic Equator. In Physics of the Hot Plasma in the Magnetosphere, ed. Bengt Hultqvist and Lennart Stenflo, Plenum Press, 91, 1975.

McIlwain, C.E., 1981. Cold Plasma Boundaries and Auroral Arcs. In Physics of Auroral Arc Formation, Geophysical Monograph Series, Vol. 25.

Paschmann, G., Melzner, F., Frenzel, R., Vaith, H., Parigger, P., Pagel, U., Bauer, O.H., Haerendel, G., Baumjohann, W., Sckopke, N., Torbert, R.B., Briggs, B., Chan, J., Lynch, K., Morey, K., Quinn, J.M., Simpson, D., Young, C., McIlwain, C.E., Fillius, W., Kerr, S.S., Maheu, R., and Whipple, E.C., 1997. The Electron Drift Instrument for Cluster. Space Sci. Rev. 79, 233.

Paschmann, G., McIlwain, C.E., Quinn, J.M., Torbert, R.B., and Whipple, E.C., 1998. The Electron Drift Technique for Measuring Electric and Magnetic Fields. In R.F. Pfaff, J.E. Borovsky and D.T. Young (eds.), Measurement Techniques in Space Plasmas – Fields. AGU Geophysical Monograph 103, 29.

Pfaff, R., Clemmons, J., Carlson, C., Ergun, R., McFadden, J., Mozer, F., Temerin, M., Klumpar, D., Peterson, W., Shelley, E., Mœbius, E., Kistler, L., Strangeway, R., Elphic, R., and Cattell, C., 1998. Initial FAST observations of acceleration processes in the cusp. Geophys. Res. Lett. 25(12), 2037.

Runov, A., Asano, Y., Vörös, Z., Nakamura, R., Baumjohann, W., Paschmann, G., Quinn, J., McIlwain, C., Balogh, A., and Rème, H., 2004. Cluster Magnetotail Probe During the 13 September 2002 Substorm. in Proc. ICS-7. 188, 2004. in press.

Shukla, P.K., Mamun, A.A., and Eliasson, B., 2004. 3D Electron-Acoustic Solitary Waves Introduced by Phase Space Electron Vortices in Magnetized Space Plasmas. Geophys. Res. Lett. 31, L07803.

Sundkvist, D., Krasnoselskikh, V., Shukla, P., Vaivads, A., André, M., Buchert, S., and Rème, H., 2005. *In Situ* Multi-Satellite Detection of Coherent Vortices as a Manifestation of Alfvénic Turbulence. Nature 436, 825, August 11, 2005.

Torrence, C., and Compo, G., 1998. A Practical Guide to Wavelet Analysis. Bull. Amer. Meteor. Soc. 79, 61.

Trattner, K.J., Fuselier, S.A., and Peterson, W.K., 2002. Spatial features observed in the cusp under steady solar wind conditions. J. Geophys. Res.

107(A10), 10-1.

Vaith, H., Frenzel, R., Paschmann, G., and Melzner, F., 1998. Electron Gyro Time Measurement Techniques for Determining Electric and Magnetic Fields. In R.F. Pfaff, J.E. Borovsky and D.T. Young (eds.), Measurement Techniques in Space Plasmas – Fields. AGU Geophysical Monograph 103, 47.